Title

People living with HIV have low trabecular bone mineral density, high bone marrow adiposity, and poor trabecular bone microarchitecture at the proximal femur

Journal

Osteoporosis International, 33(8)

ISSN

0937-941X

Authors

Carballido-Gamio, J
Posadzy, M
Wu, P-H
et al.

Publication Date

2022-08-01

DOI

10.1007/s00198-022-06405-y

Peer reviewed

HHS Public Access

Author manuscript

Osteoporos Int. Author manuscript; available in PMC 2023 August 01.

Published in final edited form as:

Osteoporos Int. 2022 August ; 33(8): 1739–1753. doi:10.1007/s00198-022-06405-y.

People Living with HIV Have Low Trabecular Bone Mineral Density, High Bone Marrow Adiposity, and Poor Trabecular Bone Microarchitecture at the Proximal Femur

Julio Carballido-Gamio, PhD[1], **Magdalena Posadzy, MD**[2], **Po-Hung Wu, PhD**[2], **Katie Kenny**[3], **Isra Saeed, MD**[2], **Thomas M. Link, MD, PhD**[2], **Phyllis C. Tien, MD**[4,5], **Roland Krug, PhD**[2], **Galateia J. Kazakia, PhD**[2]

[1]Department of Radiology, University of Colorado Anschutz Medical Campus, Aurora CO

[2]Department of Radiology and Biomedical Imaging, University of California, San Francisco, San Francisco CA

[3]Department of Bioengineering, University of California, Berkeley, Berkeley CA

[4]Department of Medicine, University of California, San Francisco, San Francisco CA

[5]Department of Veterans Affairs Medical Center, San Francisco CA

Abstract

Introduction: People living with HIV (PLWH) have increased risk of osteoporosis and fractures. However, studies assessing the main determinants of bone strength in the proximal femur exclude this vulnerable population. We assessed the proximal femur of 40 PLWH and 26 age-matched seronegative controls using quantitative computed tomography and magnetic resonance imaging.

Methods: We examined cortical volumetric bone mineral density (Ct.vBMD), trabecular vBMD (Tb.vBMD), cortical thickness (Ct.Th), bone marrow adiposity (BMA), and trabecular number, separation, and bone volume fraction. Parametric comparisons between the two groups were done for the femoral head, femoral neck, trochanter, and total hip using linear regression adjusting for several covariates, including metrics of body composition. In addition, we investigated the associations of BMA with Tb.vBMD and trabecular microarchitecture with Spearman's rank partial correlations.

Results: PLWH had lower Tb.vBMD and deteriorated trabecular microarchitecture in the femoral neck, trochanter and total hip, and elevated BMA in the femoral head, femoral neck and total hip. Ct.vBMD and Ct.Th were not significantly different between the two groups. BMA was significantly associated with lower Tb.vBMD and deteriorated trabecular microarchitecture in both groups albeit at different femoral regions.

Corresponding Author: Julio Carballido-Gamio, Assistant Professor, Department of Radiology, University of Colorado Anschutz Medical Campus, 12700 E 19th Ave, Mail Stop C278, Room 1208, Aurora CO 80045, Julio.Carballido-Gamio@cuanschutz.edu, Tel: +1 (303)-724-6153.

Conflict of Interest: Julio Carballido-Gamio, Magdalena Posadzy, Po-Hung Wu, Katie Kenny, Isra Saeed, Thomas M. Link, Phyllis C. Tien, Roland Krug, and Galateia J. Kazakia declare that they have no conflict of interest.

Conclusions: Our findings suggest that the trabecular, and not the cortical, compartment is compromised in the proximal femur of PLWH. The observed impairments in fracture-prone regions in PLWH indicate lower femoral strength and suggest higher fracture risk. The inverse associations of BMA with trabecular bone density and microarchitecture quality agree with findings at other anatomic sites and in other populations suggesting that excess BMA possibly due to a switch from the osteoblast to the adipocyte lineage may be implicated in the pathogenesis of bone fragility at the femur in PLWH.

Mini Abstract

People living with HIV (PLWH) have increased risk of osteoporosis and fractures. We assessed the proximal femur of PLWH and age-matched seronegative controls using quantitative computed tomography and magnetic resonance imaging. Results suggest that the trabecular compartment is compromised at fracture-prone regions in the proximal femur of PLWH.

Keywords

HIV infection; bone mineral density; cortical bone thickness; bone marrow fat; bone microarchitecture

1. Introduction

The effectiveness of antiretroviral therapies (ARTs) has significantly increased the life expectancy in adults with human immunodeficiency virus-1 (HIV) infection. Unfortunately, the longer life-span in people living with HIV (PLWH) is accompanied by several comorbidities, including cardiovascular disease, cancer, diabetes mellitus, liver disease, and renal dysfunction [1]. Bone fragility is also being increasingly recognized as another significant comorbidity of HIV infection and treatment, with a number of cross-sectional studies reporting that PLWH have reduced spine and hip areal bone mineral density (aBMD) derived from dual-energy X-ray absorptiometry (DXA) [2-6], and meta-analyses confirming that PLWH have increased risk of fracture [7, 8].

Bone strength is determined by its density and quality, including bone microarchitecture. Although aBMD is the clinical standard to assess osteoporosis and fracture risk, aBMD is a two-dimensional (2D) parameter that cannot distinguish between cortical and trabecular bone, and does not provide bone microarchitecture, volumetric BMD (vBMD), or cortical bone thickness quantification. There is increasing evidence that HIV infection and its treatment impact the quality of bone, increasing the fracture risk of PLWH, even without changes in aBMD [9]. Most of the existing data on bone quality in PLWH comes from high-resolution peripheral quantitative computed tomography (HR-pQCT) studies assessing the distal radius and tibia [9-13]. However, the proximal femur is an important anatomical site for fracture, as femoral fractures are usually accompanied with high morbidity and mortality. Central QCT offers the capability to perform 3D assessments of compartmental vBMD – i.e., trabecular and cortical vBMD – and cortical bone thickness at the proximal femur. Magnetic resonance imaging (MRI) is the only imaging modality enabling the in-vivo visualization and quantification of trabecular bone microarchitecture at the proximal femur. Furthermore, MRI enables accurate in-vivo assessments of bone marrow adiposity (BMA),

essential for examining the etiology of bone fragility [14]. Nevertheless, studies taking advantage of the 3D capabilities of QCT and MRI [9] to assess determinants of bone strength at the proximal femur and improve our understanding of bone fragility in PLWH are limited. In fact, to the best of our knowledge, there are no QCT studies assessing the proximal femur of PLWH.

The association of BMA with lower BMD [15], and the evidence that BMA increases with age [16, 17], menopause [18] and osteoporosis [19, 20], as well as decreasing in response to osteoporosis treatments [21, 22], have resulted in studies investigating BMA as an imaging biomarker of bone fragility. In addition to the well-established magnetic resonance spectroscopy (MRS) techniques, which enable assessments of bone marrow fat content and composition within low-spatial resolution volumes of interest, recent advances in MRI pulse sequence development and reconstruction algorithms now enable fast and accurate spatial assessments of BMA with high-spatial resolution using chemical-shift encoding-based water-fat separation techniques [23, 24]. These techniques generate an image, which is a proton density fat fraction (PDFF) map, i.e., a spatial representation of the signal arising from fat protons divided by the sum of the signals from fat and water protons. BMA assessments derived from chemical-shift encoding-based water-fat separation techniques have been proven to be as accurate as those derived from MRS at the proximal femur [23], and have been validated with cadaveric trabecular bone phantoms where the marrow spaces were filled with water-fat gelatin of known fat fractions [24]. While studies have reported an inverse association between BMA and BMD [14, 15, 25], this association has not been fully explored at the proximal femur, especially in PLWH. Furthermore, the associations of BMA with trabecular bone microarchitecture at the proximal femur are completely unknown.

The aim of this study was to perform a comprehensive multiparametric assessment of bone density, quality, and marrow adiposity at the proximal femur in PLWH to improve our understanding of bone fragility in this vulnerable population. We used QCT to measure cortical vBMD, trabecular vBMD, and cortical bone thickness, and MRI to measure BMA and trabecular bone microarchitecture in 40 PLWH and 26 age-matched seronegative (SN) controls. We compared bone properties between the two groups and investigated the associations of BMA with trabecular vBMD and trabecular bone microarchitecture in each group. Based on our preliminary results [9] and the scientific literature [13], we hypothesized that PLWH have lower cortical and trabecular vBMD, thinner cortical bone, greater BMA, and worse trabecular bone microarchitecture quality at the proximal femur with respect to SN controls. We also hypothesized that BMA is inversely related to trabecular vBMD and quality of trabecular bone microarchitecture in both PLWH and SN controls.

2. Materials and Methods

The current HIPAA compliant study was approved by the institutional review boards of the participating institutions and conducted in accordance with their regulations. Informed consent was obtained from all participants in the study, and the analyses were performed on de-identified data.

2.1 Study Participants

This cross-sectional study included 40 PLWH and 26 SN controls. Participants were recruited over a 4-year period from the UCSF and San Francisco community, and via targeted recruitment through 1) the UCSF 360: Positive Care Center, 2) Zuckerberg San Francisco General Hospital, and 3) the Women's Interagency HIV study (WIHS) participant cohort. The target age range for enrollment was 50-70 years, and SN controls were frequency matched for age (5-year bins). All seropositive participants had known infection for ≥7 years, were on a stable tenofovir-based ART regimen in the prior year, with HIV RNA < 40 copies/ml. Participants were excluded if they were pre- or peri-menopausal (last menses ≤ 3 years), or had chronic diseases (other than HIV infection) associated with poor bone quality such as diabetes mellitus, rheumatologic diseases, chronic kidney disease, malabsorption syndromes or hepatitis C virus infection. Participants treated with medications known to impact bone and mineral metabolism, including use of bisphosphonate or teriparatide in the last year or for >12 months ever, current calcitonin, prednisone >5 mg daily or the equivalent glucocorticoid for >10 days in the last 3 months, current thiazolidinedione (TZD), thyroid hormone replacement with current thyroid stimulating hormone < 0.1 mlU/L, hormonal contraceptives, or hormone replacement were also excluded. Additional exclusion criteria included BMI>35 kg/m^2 due to MRI image quality restrictions, fracture within the previous 5 years at either hip, lumbar spine, distal tibia, or distal radius, surgery at the imaging site, an episode of immobilization lasting longer than one week in the previous six months, and conditions excluded by X-ray or MRI safety guidelines [12]. Height measured with a stadiometer, weight with a scale, and self-reported race were recorded.

2.2 Imaging

2.2.1 QCT—Bilateral hip acquisitions for all participants were done with a GE CT scanner (GE Light Speed VCT; GE Medical Systems, Wakesha, WI, USA) for vBMD and cortical bone thickness quantification. Patients were in supine position and images were obtained from the top of the acetabulum to 3 cm below the lesser trochanter. A calibration phantom (Mindways Software, Austin, TX, USA) was placed under the CT table at the time of scanning to calibrate the scans to equivalent concentrations of K_2HPO_4 in mg/cm^3. The scanning protocol was 120 kVp, 200 mAs, 50 × 50 cm^2 field of view (FOV), matrix size of 512 × 512, standard reconstruction kernel, and an average of 101 slices per participant. Images were reconstructed to voxel sizes of 0.977 × 0.977 × 1.25 mm^3.

QCT scans for body composition assessments were also obtained as single 10-mm thick acquisitions in the abdominal area (mid-L4 vertebra) and mid-thigh with 120kVp, 300 mAs, 50 × 50 cm^2 FOV, matrix size of 512 × 512, and the standard soft tissue reconstruction filter. The full QCT acquisition time was ~10 minutes.

2.2.2 MRI—Images of the non-dominant proximal femur were obtained for all participants with a 3 Tesla GE MRI scanner (Discovery MR 750; GE Medical Systems, Wakesha, WI, USA). Coronal-oblique images for clinical, BMA, and trabecular bone microarchitecture assessments were obtained.

For clinical assessments, 3D fast spin echo images with T_2 weighting were obtained using a GE CUBE sequence. Imaging parameters included TR = 1,200 ms, TE = 20 ms, FOV = 15.3 × 15.3 cm^2, receiver bandwidth = 50 kHz, frequency direction = S/I, number of averages = 1, slice thickness = 0.8 mm, and a matrix size of 192 × 192 yielding isotropic voxel sizes of 0.8 ×0.8 × 0.8 mm^3, with ~7 minutes of acquisition time.

For BMA quantification, chemical shift-based water-fat separation was used based on a 3D spoiled gradient-recalled echo (SPGR) sequence with six echoes and an iterative decomposition of water and fat with echo asymmetry and least-squares estimation (IDEAL) reconstruction algorithm [23]. Imaging parameters included TR = 8.616 ms, TE/ΔTE = 3.246/1.0 ms, FOV = 12 × 12 cm^2, receiver bandwidth = 62.5 kHz, frequency direction = S/I, no phase-wrap on, number of averages = 1, a flip angle of 3° to minimize T_1-bias effects [23], slice thickness = 1.5 mm, and a final in-plane voxel size of 0.469 × 0.469 mm^2, with ~4 minutes of acquisition time.

For trabecular bone microarchitecture quantification, high-spatial resolution MR images of the proximal femur were acquired using a 3D fully balanced steady-state free precession (bSSFP) pulse sequence with two phase-cycled acquisitions. Imaging parameters included a TR = 13.216 ms, TE = 4.576 ms, flip angle = 60°, FOV = 12 × 12 cm^2, acquisition matrix = 512 × 512, slice thickness = 0.5 mm, and a final in-plane spatial resolution of 0.234 × 0.234 mm^2, with ~20 minutes of acquisition time.

2.2.3 DXA—

DXA acquisitions were also performed to assess total hip and femoral neck aBMD using a Horizon A scanner (Hologic, Marlborough, MA, USA). Areal BMD was measured in g/cm^2 and T- and Z-scores were provided.

2.3 Image Analysis

2.3.1 QCT – vBMD and Cortical Bone Thickness—

After image calibration, the analysis of QCT scans was performed using the pipeline described by Carballido-Gamio et al. [26] which enables the automatic segmentation of proximal femora and cortical bone, quantification of vBMD and cortical bone thickness (Ct.Th), and prescription of volumes of interest defining the femoral head, femoral neck, and trochanteric region (Figure 1A-1C). Therefore, for each participant we calculated cortical vBMD (Ct.vBMD; mg/cm^3), trabecular vBMD (Tb.vBMD; mg/cm^3), integral vBMD (Int.vBMD, i.e., Ct.vBMD and Tb.vBMD; mg/cm^3), and Ct.Th (mm) for the femoral head, femoral neck, trochanteric region, and total hip (femoral head, femoral neck and trochanteric region). The reproducibility of the vBMD and cortical bone thickness assessments as implemented in this study, and expressed as CV_{RMS}, are under 1.7% and 2.7%, respectively [26].

Visceral adipose tissue (VAT), abdominal subcutaneous adipose tissue (Ab-SAT), and thigh SAT areas were computed using software developed at the University of California, San Francisco. VAT was manually distinguished from SAT by tracing along the fascial plane defining the internal abdominal wall. Adipose areas in cm^2 were calculated by multiplying the number of pixels by the pixel area [27].

2.3.2 MRI – BMA and Trabecular Bone Microarchitecture—PDFF maps representing BMA were automatically computed in the MRI console using the IDEAL algorithm [28]. The reconstruction accounted for multiple peaks in the fat spectrum and performed T_2*[29] and T_1 corrections [23]. PDFF maps were exported for analyses (Figure 1D). The QCT femoral segmentations, cortical bone segmentations, and volumes of interest were transferred to the BMA maps and high-spatial resolution scans using image registration, effectively enabling multiparametric assessments from different imaging modalities at corresponding anatomical regions across all participants in the study. To make sure that BMA and trabecular bone microarchitecture assessments did not include cortical bone, we dilated (~1.6 mm) the cortical bone segmentations to remove the outer layers of the trabecular bone compartment in the MRI scans (Figures 1D-1I). Automatic coil correction by nonparametric nonuniform intensity normalization (N3) [30] was applied to the high-spatial resolution scans optimizing the proximal femur by providing the femoral segmentations to the N3 algorithm. Trabecular bone was then segmented from the N3-corrected high-spatial resolution scans using a new segmentation approach based on multi-scale structural filtering and adaptive thresholding. Briefly, multiscale bone enhancement was performed as previously described by Folkesson et al. (3 scales) [31]. Bone enhancement features at each scale were then thresholded with a 3D adaptive algorithm using local first-order statistics [32], and the results were aggregated to generate a binary representation of the trabecular bone microarchitecture (Figure 1I). For each participant, we calculated mean BMA (%), trabecular number (Tb.N; 1/mm) [33], trabecular separation (Tb.Sp; mm) [33], and trabecular bone volume fraction (Tb.BVF; unitless) for the femoral head, femoral neck, trochanteric region, and total hip. The reproducibility of BMA measurements, expressed as an absolute precision error for the proton density fat fraction, has been reported in the range of 1.45% for the lumbar vertebral bodies [34, 35], while the CV_{RMS} for Tb.BVF using a bone-enhancement fuzzy clustering technique – with the same multi-scale structural filtering as in the algorithm used in this study – was reported as 2% [31].

2.4 Statistical Analysis

Statistical analysis was performed using MATLAB (The MathWorks, Inc. Natick, MA, USA) and R. Participant characteristics were compared between the two groups using Mann-Whitney tests for continuous variables and Fisher's exact tests for categorical variables. QCT, MRI and DXA parametric comparisons were performed for each femoral region using linear regression models with imaging parameters as the dependent variable, HIV status as the independent variable, and height, sex, race (White, Asian, Black, Unknown/Not reported), VAT, and Ab-SAT as covariates. The purpose of the adipose tissue covariates was to adjust for body composition differences including lipodystrophy secondary to HIV-infection and ART [36]. In addition, adjusting for VAT and Ab-SAT, instead of BMI, allows us to take into account both differences in weight and differences in the distribution of weight. The associations of BMA with trabecular vBMD and each parameter assessing trabecular bone microarchitecture (Tb.N, Tb.Sp, Tb.BVF) were evaluated within each group using Spearman's rank partial correlations adjusting for height, sex, race (White, Asian, Black, Unknown/No-reported), VAT, and Ab-SAT. Differences in the strength of the correlation coefficients between the two groups were evaluated using the

Fisher's z transformation. Statistical analyses were computed with a two-sided 0.05 level of significance.

3. Results

The quality control assessments for the QCT and MRI acquisitions yielded two corrupted BMA maps (both from the PLWH group), and 13 high-spatial resolution MR images with motion or noise artifacts (7 PLWH and 6 SN controls) that had to be excluded from the analyses. In addition, there was one DXA scan missing (from the PLWH group). All QCT scans were deemed to be of good quality for analysis. Race was unknown or not reported for 2 SN controls and 4 PLWH. Table 1 shows the participant characteristics for the 26 SN participants and 40 PLWH included in this study. None of the participants have a history of hip fracture. Only VAT between the two groups or their subsets (due to the exclusion of unusable MRI or DXA scans) manifested significant differences. A sensitivity analysis comparing the variables listed in Table 1 between participants included and excluded in the BMA, trabecular bone microarchitecture, and correlation assessments (Appendix Table 6) yielded non-significant differences.

Table 2 summarizes the results for DXA aBMD, while Table 3 summarizes the results for QCT vBMD and cortical bone thickness. PLWH had significantly lower total hip aBMD, trabecular vBMD at the femoral neck, trochanteric region and total hip, and integral vBMD at the trochanteric region. However, none of the QCT parameters were significantly different between the two groups at the femoral head, and none of the cortical bone parameters (Ct.vBMD and Ct.Th) yielded significant differences between the two groups at any region.

With respect to BMA, PLWH had significantly elevated BMA at the femoral head, femoral neck and total hip, but not at the trochanteric region, where only a trend of elevated BMA values was observed (Table 4).

Results for trabecular bone microarchitecture are summarized in Table 4, where it can be observed that PLWH had significantly lower trabecular number at the femoral neck, significantly higher trabecular separation at the femoral neck and trochanteric region, and significantly lower trabecular bone volume fraction at the trochanteric region and total hip, but no significant differences in trabecular bone microarchitecture at the femoral head with respect to SN controls.

Table 5 summarizes the partial correlations of BMA with trabecular vBMD and trabecular bone microarchitecture parameters for each group, as well as the differences in the strength of the correlation coefficients between the two groups. BMA was significantly negatively correlated with trabecular vBMD in the femoral head and neck of SN controls, and in the femoral neck, trochanteric region, and total hip of PLWH. However, the correlations were only significantly different between the two groups (stronger in SN controls) in the femoral head. BMA also manifested significant associations with trabecular bone microarchitecture in the femoral neck of SN controls (Tb.N), and in the trochanteric region (Tb.N, Tb.Sp, and Tb.BVF) and total hip (Tb.N, Tb.Sp, and Tb.BVF) of PLWH. These associations were negative with trabecular number and bone volume fraction, and positive with trabecular

bone separation. However, the strengths of the associations of BMA with trabecular bone microarchitecture were not significantly different between the two groups.

4. Discussion

To identify appropriate interventions to prevent or mitigate HIV-related bone fragility it is necessary to understand the pathophysiology underlying bone density, quality and microenvironmental changes in this vulnerable population. In this study, we used QCT and MRI to perform 3D comprehensive multiparametric assessments of the proximal femur in PLWH and SN controls. These assessments included vBMD, cortical bone thickness, trabecular bone microarchitecture, and BMA. Our analyses showed that PLWH have significantly lower trabecular vBMD, worse trabecular bone microarchitecture, and greater BMA compared to SN controls, and that these impairments are spatially heterogenous. Our results also showed that BMA is significantly correlated with trabecular bone impairments, i.e., low trabecular vBMD and bone quality. However, the significance of these associations and their strength differed by region between the two groups. We hypothesized that PLWH have lower cortical and trabecular vBMD, thinner cortical bone, greater BMA, and worse trabecular bone microarchitecture quality at the proximal femur with respect to SN controls. We also hypothesized that BMA is inversely related to trabecular vBMD and quality of trabecular bone microarchitecture in both PLWH and SN controls. Therefore, findings reported in this study validated most of our hypotheses, except for the cortical bone assessments.

The literature addressing fracture risk in PLWH is mostly based on DXA-derived aBMD. While several studies have reported reduced aBMD in PLWH [37], only four of 11 women with HIV and fractures had osteoporotic aBMD values in the study of McComsey et al. [38] Furthermore, in the study of Prior and colleagues [39] women with HIV (n=138) had an increased incidence of fragility fractures despite similar aBMD as controls (n=402). Similarly, although our results showed that PLWH had significantly lower total hip aBMD than SN controls, femoral neck aBMD was similar between the two groups. By contrast, our QCT analysis showed that PLWH have significantly lower femoral neck Tb.vBMD. These findings suggest that QCT may be a more accurate imaging modality to investigate the etiology of bone fragility. With respect to cortical vBMD, our results were unexpected. Based on most of the DXA literature reporting reduced hip aBMD in PLWH, we hypothesized that both cortical and trabecular vBMD would be reduced in PLWH. As this is the first study to measure vBMD in the proximal femur of PLWH, we cannot compare our results to other studies. To our knowledge, only two other studies have assessed vBMD with QCT in PLWH but in the lumbar [40] and thoracic [41] spine. In the longitudinal study of Grund et al., 12-month decreases in lumbar spine trabecular vBMD (L2-L4) were reported in response to continuous ART [40], while in the cross-sectional study of Thomsen et al., HIV status was not associated with thoracic vBMD (three consecutive thoracic vertebrae starting with the vertebra in level with left main coronary artery) in univariable or multivariable linear analyses [41]. However, our QCT findings underscore the relevance of 3D compartmental vBMD analyses, and by showing reduced trabecular vBMD in fracture-prone regions (femoral neck and trochanter), our study provides a partial explanation of the increased bone fragility reported in PLWH [7, 8].

As bone strength is determined by its mineral density, quality, and microenvironment, and studies have reported increased fracture risk in PLWH even without changes in aBMD [9], we hypothesized that bone microarchitecture – a factor of bone quality – and bone marrow adiposity – a component of the bone microenvironment – should play central roles on bone fragility in this population. The scientific literature addressing the associations of BMA with HIV infection is limited to two studies. Huang et al. used MRS to measure intravertebral BMA (L3-L5) in 15 men with HIV (39±5 years) and 9 age- and BMI-matched healthy control participants (39±8 years) [42]. The authors reported that intravertebral BMA was significantly lower in the group with HIV (28.5±8.0 %) compared with SN controls (37.3±12.5 %). Interestingly, the authors also reported significantly lower lumbar spine aBMD in the group with HIV. In the second study – by the same group of researchers – proton spectroscopic imaging was used to assess vertebral BMA (L3-L5) in 20 men with HIV (38.5±5.2 years) and 15 men without HIV (36.7±8.0 years) [43]. The investigators again reported lower BMA in the group with HIV (29±8 %) compared to those without HIV (40±12 %). The findings of these two studies are in contrast to published studies in other non-HIV patient cohorts showing an inverse association of high BMA with low bone density and quality. They are also in conflict with our findings, which show that PLWH have higher BMA than SN controls at the proximal femur. When interpreting this discrepancy, it is important to note that in the other two studies as well as this study, BMA was of the *regulated* type (lumbar spine, femur and proximal tibia), which is more dynamic and responsive to hormonal and nutritional changes than *constitutive* BMA (distal tibia) [14]. This discrepancy could be due in part to differences in the characteristics of the participants (older men and women in our study vs. young men in the other), time on stable ART regimen (≥ 1 year vs. ≥12 weeks), type of ART regimen (tenofovir-based ART vs. not reported) time of infection (≥7 years vs. not reported), statistical analyses (adjustments for several covariates vs. no adjustments), or to the number of participants (38 PLWH and 26 SN controls vs. 15 PLWH and 9 SN controls vs. 20 PLWH and 15 SN controls). However, our results are in agreement with the literature on aging, osteoporosis and fracture risk, where an imbalance of stromal cell lineage determination in favor of increased adipogenesis and decreased osteoblastogenesis has been reported [44, 45]. Furthermore, in the setting of HIV infection, the HIV virus interferes with β-catenin in the Wnt signaling pathway responsible for stromal cell lineage determination [46]. The inhibition of the Wnt pathway alters the balance of common progenitor lineage determination in favor of increased adipogenesis and decreased osteoblastogenesis [47], which would lead to increased BMA and impairments in bone microarchitecture.

In terms of bone microarchitecture, there are no studies in the literature reporting cortical bone thickness in the proximal femur of PLWH, and the only existing study assessing trabecular bone microarchitecture in the proximal femur of PLWH is from our research group. In our previous work, we reported trabecular bone microarchitecture impairments in men with HIV (n=8) compared with SN control men (n=11) at different femoral regions. However, these impairments were attenuated and no longer significant after adjusting for BMI [9]. In the current study, we also identified trabecular bone microarchitecture impairments in PLWH at different femoral regions. However, these impairments prevailed even after adjustments for several covariates, including metrics of body composition. It is

interesting to note that BMA and microarchitectural analyses were also performed without adjustments for VAT and Ab-SAT yielding different *P*-values, but without changes in the significance of the results. While studies assessing bone quality at the proximal femur of PLWH are limited, we identified four studies investigating bone microarchitecture at the distal extremities of older PLWH using HR-pQCT. However, these studies have reported conflicting results. In a study of postmenopausal Hispanic and African American women with (n=46) and without (n=60) HIV, Yin et al. reported that lower cortical bone thickness and area at the tibia were the only differences detected between the two groups [10]. In contrast, in the cross-sectional study of Biver et al., in addition to lower cortical area at the distal tibia, HIV-positive men (n=28) had lower total vBMD and trabecular vBMD at the distal tibia, and lower total vBMD, trabecular vBMD, trabecular number, cortical thickness and area, and higher trabecular separation at the distal radius compared with HIV-negative men (n=112) [11]. In a more recent study by Kazakia et al., men with HIV (n=20) showed significantly lower trabecular number and higher trabecular separation at both the distal radius and tibia compared with age- and BMI-matched uninfected control men (n=18) [9]. And in the most recent study by Macdonald et al., postmenopausal women living with HIV (n=50) showed lower trabecular vBMD and thickness at the distal radius, and lower trabecular vBMD at the distal tibia compared with SN controls (n=50). No significant differences in cortical vBMD and area were detected between the two groups [13]. Nevertheless, results of our bone quality analyses indicate that PLWH manifest trabecular bone microarchitecture impairments at fracture-prone regions (the femoral neck and trochanteric regions). As these regions also showed impairments in trabecular vBMD and BMA in PLWH, our study provides unique and novel data to explain the bone fragility observed in PLWH [7, 8]. As HIV studies with larger sample sizes report impairments of trabecular bone microarchitecture in the proximal femur of PLWH – especially in the presence of non-osteoprotic T-scores – MRI-based trabecular bone microarchitectural assessments might become clinically relevant.

The directionality of the associations of BMA with trabecular vBMD and bone microarchitecture yielded by the partial correlation analyses was as expected [14, 15, 25], i.e., BMA was negatively associated with Tb.vBMD and improved trabecular bone microarchitecture. The most interesting findings in these analyses were the differences in strength of the associations at each femoral region – albeit not significant – between the two groups. These results indicate spatially differential effects of HIV infection on vBMD, trabecular bone microarchitecture, and BMA. Additional observations were the lack of significant associations of BMA with trabecular bone microarchitecture at the femoral head in both groups – perhaps due to the modest sample sizes – and the differences in strength of the associations between femoral regions within each group. These within-group differences could be partly explained by the structural adaptation of the proximal femur to sustain the most common loading conditions in daily life such as standing and walking. This adaptation translates into a much thicker inferior than superior cortex [48], and a trabecular network positioned to resist and transmit weight-bearing directed loads [49, 50]. The associations of BMA with trabecular vBMD and trabecular bone microarchitecture are therefore expected to be spatially heterogenous. These results also suggest that BMA provides information independent of trabecular vBMD and bone microarchitecture and underscore the relevance

of spatial assessments in addition to global analyses to improve our understanding of bone fragility in this vulnerable population.

This study has several strengths. This is the first study to simultaneously assess key determinants of bone strength (density, quality, and microenvironment) in the same individuals and at an anatomical site of utmost importance with respect to osteoporosis assessment and fracture risk, i.e., the proximal femur. This is also the first study to assess vBMD, cortical bone thickness and BMA at the proximal femur in PLWH, and the first study to explore the associations of BMA with trabecular vBMD and microarchitecture at the proximal femur. However, this study also has four major limitations. First, its cross-sectional nature limited our interpretations to associations instead of causations. Second, the imbalance in the number of women and men between the two groups (54% women in the SN group vs. 30% in the PLWH group) made us adjust for sex in our statistical analyses, and precluded analyses stratified by sex, which might be relevant particularly for BMA as this has been shown to increase in women during menopause [18]. Third, with the majority of participants being recruited from the San Francisco Bay Area, our results may not be generalizable to other populations, including other ethnicities or even other white groups with different characteristics. And fourth, the modest sample sizes impacted the power of the study, and due to the large number of imaging parameters, we decided a priori not to correct for multiple comparisons. Therefore, results should be interpreted with caution.

5. Conclusions

In conclusion, in this multiparametric and multimodality imaging study we observed that PLWH had lower trabecular vBMD, worse trabecular bone microarchitecture, and higher BMA at fracture-prone regions in the proximal femur compared to SN controls. We also showed that BMA was significantly associated with lower trabecular vBMD and worse trabecular bone microarchitecture quality in both groups albeit at different femoral regions. Our findings suggest that the trabecular, and not the cortical, compartment is compromised in the proximal femur of PLWH. The observed bone impairments in fracture-prone regions in PLWH are indicators of lower femoral strength, suggesting a higher fracture risk in this vulnerable population. The inverse associations of BMA with trabecular bone density and microarchitecture quality are consistent with findings from other studies at other anatomic sites and in other populations and suggest that excess marrow fat possibly due to a switch from the osteoblast to the adipocyte lineage may be implicated in the pathogenesis of bone fragility at the femur in PLWH. Future work will assess the associations between BMA and BMA heterogeneity with body composition (VAT/SAT) to understand if BMA changes in HIV are driven by HIV-associated lipodystrophy, as well as to understand the differential effects of HIV on bone parameters with respect to bone strength.

Acknowledgements

This study was supported by NIH NIAID R01 AI125080, NIH NIAMS P30 DK098722 (NORC), and NIH NIAMS P30AR075055.

Data Availability

Please direct any data requests to the Principal Investigators of this study:

Dr. Galateia J. Kazakia: Galateia.Kazakia@ucsf.edu

Dr. Roland Krug: Roland.Krug@ucsf.edu

Appendix

Table 6.

Characteristics of the excluded participants for the different analyses in this study.

Participants excluded for BMA adiposity assessments.		
	SN controls	**PLWH**
n	0	2
Age (years)		58 (54-62)
Height (cm)		167.10 (156.40-177.80)
Weight (kg)		81.38 (67.50-95.25)
BMI (kg/m^2)		28.66 (27.59-30.13)
VAT (cm^2)		133.06 (99.46-166.65)
Ab-SAT (cm^2)		353.83 (250.76-456.90)
Thigh-SAT (cm^2)		88.13 (48.28-127.99)
Normal T-score		1
Osteopenic T-score		1
Osteoporotic T-score		0
Absolute CD4 count (cells/uL)		1097 (491-1703)
Sex		1 female
Race - White		2
Race - Black		0
Race - Asian		0
Race - Unknown/Not reported		0

Participants excluded for trabecular bone assessments.		
	SN controls	**PLWH**
n	6	7
Age (years)	53.50 (50.00-67.00)	55.00 (52.00-66.00)
Height (cm)	170.50 (160.90-180.10)	166.40 (156.40-180.20)
Weight (kg)	72.10 (58.20-101.20)	70.31 (54.00-112.60)
BMI (kg/m^2)	25.47 (21.15-31.20)	27.59 (20.73-34.68)
VAT (cm^2)	116.52 (32.09-174.12)	151.96 (54.24-266.47)
Ab-SAT (cm^2)	186.82 (57.13-454.68)	271.99 (91.64-459.04)
Thigh-SAT (cm^2)	72.28 (39.21-125.56)	48.28 (25.58-129.27)
Normal T-score	5	3
Osteopenic T-score	1	4
Osteoporotic T-score	0	0

Participants excluded for trabecular bone assessments.

	SN controls	PLWH
Absolute CD4 count (cells/uL)		757 (472-1052)
Sex	4 females	4 females
Race - White	3	3
Race - Black	1	2
Race - Asian	1	0
Race - Unknown/Not reported	1	2

Participants excluded for partial correlation assessments.

	SN controls	PLWH
n	6	8
Age (years)	53.50 (50.00-67.00)	54.50 (52.00-66.00)
Height (cm)	170.50 (160.90-180.10)	168.05 (156.40-180.20)
Weight (kg)	72.10 (58.20-101.20)	75.25 (54.00-112.60)
BMI (kg/m^2)	25.47 (21.15-31.20)	27.72 (20.73-34.68)
VAT (cm^2)	116.52 (32.09-174.12)	159.31 (54.24-266.47)
Ab-SAT (cm^2)	186.82 (57.13-454.68)	284.76 (91.64-459.04)
Thigh-SAT (cm^2)	72.28 (39.21-125.56)	85.97 (25.58-129.27)
Normal T-score	5	3
Osteopenic T-score	1	5
Osteoporotic T-score	0	0
Absolute CD4 count (cells/uL)		792.50 (472-1703)
Sex	4 females	4 females
Race - White	3	4
Race - Black	1	2
Race - Asian	1	0
Race - Unknown/Not reported	1	2

No significant differences were identified between the included and excluded participants using Mann-Whitney tests for continuous variables and Fisher's exact test for T-score levels, sex, and race.

References

1. Compston J, HIV infection and bone disease," J Intern Med, vol. 280, no. 4, pp. 350–8, Oct 2016, doi: 10.1111/joim.12520. [PubMed: 27272530]
2. Knobel H, Guelar A, Vallecillo G, Nogues X, and Diez A, "Osteopenia in HIV-infected patients: is it the disease or is it the treatment?," AIDS, vol. 15, no. 6, pp. 807–8, Apr 13 2001, doi: 10.1097/00002030-200104130-00022. [PubMed: 11371701]
3. Bruera D, Luna N, David DO, Bergoglio LM, and Zamudio J, "Decreased bone mineral density in HIV-infected patients is independent of antiretroviral therapy," AIDS, vol. 17, no. 13, pp. 1917–23, Sep 5 2003, doi: 10.1097/00002030-200309050-00010. [PubMed: 12960824]
4. Dolan SE, Huang JS, Killilea KM, Sullivan MP, Aliabadi N, and Grinspoon S, "Reduced bone density in HIV-infected women," AIDS, vol. 18, no. 3, pp. 475–83, Feb 20 2004, doi: 10.1097/00002030-200402200-00014. [PubMed: 15090800]
5. Yin M et al. , "Bone mass and mineral metabolism in HIV+ postmenopausal women," Osteoporos Int, vol. 16, no. 11, pp. 1345–52, Nov 2005, doi: 10.1007/s00198-005-1845-0. [PubMed: 15754081]

6. Arnsten JH, Freeman R, Howard AA, Floris-Moore M, Santoro N, and Schoenbaum EE, "HIV infection and bone mineral density in middle-aged women," Clin Infect Dis, vol. 42, no. 7, pp. 1014–20, Apr 1 2006, doi: 10.1086/501015. [PubMed: 16511769]
7. Shiau S, Broun EC, Arpadi SM, and Yin MT, "Incident fractures in HIV-infected individuals: a systematic review and meta-analysis," AIDS, vol. 27, no. 12, pp. 1949–57, Jul 31 2013, doi: 10.1097/QAD.0b013e328361d241. [PubMed: 24126140]
8. Premaor MO and Compston JE, "The Hidden Burden of Fractures in People Living With HIV," JBMR Plus, vol. 2, no. 5, pp. 247–256, Sep 2018, doi: 10.1002/jbm4.10055. [PubMed: 30283906]
9. Kazakia GJ et al. , "Trabecular bone microstructure is impaired in the proximal femur of human immunodeficiency virus-infected men with normal bone mineral density," Quant Imaging Med Surg, vol. 8, no. 1, pp. 5–13, Feb 2018, doi: 10.21037/qims.2017.10.10. [PubMed: 29541618]
10. Yin MT et al. , "Trabecular and cortical microarchitecture in postmenopausal HIV-infected women," Calcif Tissue Int, vol. 92, no. 6, pp. 557–65, Jun 2013, doi: 10.1007/s00223-013-9716-8. [PubMed: 23460340]
11. Biver E, Calmy A, Delhumeau C, Durosier C, Zawadynski S, and Rizzoli R, "Microstructural alterations of trabecular and cortical bone in long-term HIV-infected elderly men on successful antiretroviral therapy," AIDS, vol. 28, no. 16, pp. 2417–27, Oct 23 2014, doi: 10.1097/qad.0000000000000445. [PubMed: 25389553]
12. Foreman SC et al. , "Factors associated with bone microstructural alterations assessed by HR-pQCT in long-term HIV-infected individuals," Bone, vol. 133, p. 115210, Apr 2020, doi: 10.1016/j.bone.2019.115210. [PubMed: 31874226]
13. Macdonald HM et al. , "Deficits in bone strength, density and microarchitecture in women living with HIV: A cross-sectional HR-pQCT study," Bone, vol. 138, p. 115509, Sep 2020, doi: 10.1016/j.bone.2020.115509. [PubMed: 32599222]
14. Singhal V et al. , "Differential associations between appendicular and axial marrow adipose tissue with bone microarchitecture in adolescents and young adults with obesity," Bone, vol. 116, pp. 203–206, Nov 2018, doi: 10.1016/j.bone.2018.08.009. [PubMed: 30107255]
15. Schwartz AV, "Marrow fat and bone: review of clinical findings," Front Endocrinol (Lausanne), vol. 6, p. 40, 2015, doi: 10.3389/fendo.2015.00040. [PubMed: 25870585]
16. Justesen J, Stenderup K, Ebbesen EN, Mosekilde L, Steiniche T, and Kassem M, "Adipocyte tissue volume in bone marrow is increased with aging and in patients with osteoporosis," Biogerontology, vol. 2, no. 3, pp. 165–71, 2001, doi: 10.1023/a:1011513223894. [PubMed: 11708718]
17. Griffith JF, Yeung DK, Ma HT, Leung JC, Kwok TC, and Leung PC, "Bone marrow fat content in the elderly: a reversal of sex difference seen in younger subjects," J Magn Reson Imaging, vol. 36, no. 1, pp. 225–30, Jul 2012, doi: 10.1002/jmri.23619. [PubMed: 22337076]
18. Kawai M, de Paula FJ, and Rosen CJ, "New insights into osteoporosis: the bone-fat connection," J Intern Med, vol. 272, no. 4, pp. 317–29, Oct 2012, doi: 10.1111/j.1365-2796.2012.02564.x. [PubMed: 22702419]
19. Yeung DK, Griffith JF, Antonio GE, Lee FK, Woo J, and Leung PC, "Osteoporosis is associated with increased marrow fat content and decreased marrow fat unsaturation: a proton MR spectroscopy study," J Magn Reson Imaging, vol. 22, no. 2, pp. 279–85, Aug 2005, doi: 10.1002/jmri.20367. [PubMed: 16028245]
20. Griffith JF et al. , "Vertebral marrow fat content and diffusion and perfusion indexes in women with varying bone density: MR evaluation," Radiology, vol. 241, no. 3, pp. 831–8, Dec 2006, doi: 10.1148/radiol.2413051858. [PubMed: 17053202]
21. Duque G, Li W, Adams M, Xu S, and Phipps R, "Effects of risedronate on bone marrow adipocytes in postmenopausal women," Osteoporos Int, vol. 22, no. 5, pp. 1547–53, May 2011, doi: 10.1007/s00198-010-1353-8. [PubMed: 20661545]
22. Yang Y et al. , "Effect of zoledronic acid on vertebral marrow adiposity in postmenopausal osteoporosis assessed by MR spectroscopy," Skeletal Radiol, vol. 44, no. 10, pp. 1499–505, Oct 2015, doi: 10.1007/s00256-015-2200-y. [PubMed: 26130070]
23. Karampinos DC, Melkus G, Baum T, Bauer JS, Rummeny EJ, and Krug R, "Bone marrow fat quantification in the presence of trabecular bone: initial comparison between water-fat imaging

and single-voxel MRS," Magn Reson Med, vol. 71, no. 3, pp. 1158–65, Mar 2014, doi: 10.1002/mrm.24775. [PubMed: 23657998]

24. Gee CS et al. , "Validation of bone marrow fat quantification in the presence of trabecular bone using MRI," J Magn Reson Imaging, vol. 42, no. 2, pp. 539–44, Aug 2015, doi: 10.1002/jmri.24795. [PubMed: 25425074]
25. Bredella MA et al. , "Determinants of bone microarchitecture and mechanical properties in obese men," J Clin Endocrinol Metab, vol. 97, no. 11, pp. 4115–22, Nov 2012, doi: 10.1210/jc.2012-2246. [PubMed: 22933540]
26. Carballido-Gamio J et al. , "Automatic multi-parametric quantification of the proximal femur with quantitative computed tomography," Quant Imaging Med Surg, vol. 5, no. 4, pp. 552–68, Aug 2015, doi: 10.3978/j.issn.2223-4292.2015.08.02. [PubMed: 26435919]
27. Murphy RA et al. , "Adipose tissue density, a novel biomarker predicting mortality risk in older adults," J Gerontol A Biol Sci Med Sci, vol. 69, no. 1, pp. 109–17, Jan 2014, doi: 10.1093/gerona/glt070. [PubMed: 23707956]
28. Reeder SB et al. , "Iterative decomposition of water and fat with echo asymmetry and least-squares estimation (IDEAL): application with fast spin-echo imaging," Magn Reson Med, vol. 54, no. 3, pp. 636–44, Sep 2005, doi: 10.1002/mrm.20624. [PubMed: 16092103]
29. Yu H et al. , "Multiecho reconstruction for simultaneous water-fat decomposition and T2* estimation," J Magn Reson Imaging, vol. 26, no. 4, pp. 1153–61, Oct 2007, doi: 10.1002/jmri.21090. [PubMed: 17896369]
30. Sled JG, Zijdenbos AP, and Evans AC, "A nonparametric method for automatic correction of intensity nonuniformity in MRI data," IEEE Trans Med Imaging, vol. 17, no. 1, pp. 87–97, Feb 1998, doi: 10.1109/42.668698. [PubMed: 9617910]
31. Folkesson J, Carballido-Gamio J, Eckstein F, Link TM, and Majumdar S, "Local bone enhancement fuzzy clustering for segmentation of MR trabecular bone images," Med Phys, vol. 37, no. 1, pp. 295–302, Jan 2010, doi: 10.1118/1.3264615. [PubMed: 20175492]
32. Bradley D and Roth G, "Adaptive Thresholding Using the Integral Image.," Journal of Graphics Tools, vol. 12, no. 2, pp. 13–21, 2007.
33. Majumdar S and Genant HK, "Assessment of trabecular structure using high resolution magnetic resonance imaging," Stud Health Technol Inform, vol. 40, pp. 81–96, 1997. [Online]. Available: https://www.ncbi.nlm.nih.gov/pubmed/10168884. [PubMed: 10168884]
34. Baum T et al. , "Assessment of whole spine vertebral bone marrow fat using chemical shift-encoding based water-fat MRI," J Magn Reson Imaging, vol. 42, no. 4, pp. 1018–23, Oct 2015, doi: 10.1002/jmri.24854. [PubMed: 25639780]
35. Li G et al. , "Comparison of chemical shift-encoded water-fat MRI and MR spectroscopy in quantification of marrow fat in postmenopausal females," J Magn Reson Imaging, vol. 45, no. 1, pp. 66–73, Jan 2017, doi: 10.1002/jmri.25351. [PubMed: 27341545]
36. Shlay JC et al. , "The effect of individual antiretroviral drugs on body composition in HIV-infected persons initiating highly active antiretroviral therapy," J Acquir Immune Defic Syndr, vol. 51, no. 3, pp. 298–304, Jul 1 2009, doi: 10.1097/QAI.0b013e3181aa1308. [PubMed: 19412117]
37. Premaor MO and Compston JE, "People living with HIV and fracture risk," Osteoporos Int, vol. 31, no. 9, pp. 1633–1644, Sep 2020, doi: 10.1007/s00198-020-05350-y. [PubMed: 32206852]
38. McComsey GA et al. , "Fragility fractures in HIV-infected patients: need for better understanding of diagnosis and management," J Int Assoc Physicians AIDS Care (Chic), vol. 3, no. 3, pp. 86–91, Jul-Sep 2004, doi: 10.1177/154510970400300303. [PubMed: 15573712]
39. Prior J et al. , "Fragility fractures and bone mineral density in HIV positive women: a case-control population-based study," Osteoporos Int, vol. 18, no. 10, pp. 1345–53, Oct 2007, doi: 10.1007/s00198-007-0428-7. [PubMed: 17665239]
40. Grund B et al. , "Continuous antiretroviral therapy decreases bone mineral density," AIDS, vol. 23, no. 12, pp. 1519–29, Jul 31 2009, doi: 10.1097/QAD.0b013e32832c1792. [PubMed: 19531929]
41. Thomsen MT et al. , "Prevalence of and Risk Factors for Low Bone Mineral Density Assessed by Quantitative Computed Tomography in People Living With HIV and Uninfected Controls," J Acquir Immune Defic Syndr, vol. 83, no. 2, pp. 165–172, Feb 1 2020, doi: 10.1097/QAI.0000000000002245. [PubMed: 31929404]

42. Huang JS, Mulkern RV, and Grinspoon S, "Reduced intravertebral bone marrow fat in HIV-infected men," AIDS, vol. 16, no. 9, pp. 1265–9, Jun 14 2002, doi: 10.1097/00002030-200206140-00009. [PubMed: 12045492]
43. Mulkern RV, Huang J, Vajapeyam S, Packard AB, Oshio K, and Grinspoon S, "Fat fractions and spectral T2 values in vertebral bone marrow in HIV- and non-HIV-infected men: a 1H spectroscopic imaging study," Magn Reson Med, vol. 52, no. 3, pp. 552–8, Sep 2004, doi: 10.1002/mrm.20205. [PubMed: 15334574]
44. Rosen CJ and Bouxsein ML, "Mechanisms of disease: is osteoporosis the obesity of bone?," Nat Clin Pract Rheumatol, vol. 2, no. 1, pp. 35–43, Jan 2006, doi: 10.1038/ncprheum0070. [PubMed: 16932650]
45. Sadie-Van Gijsen H, Hough FS, and Ferris WF, "Determinants of bone marrow adiposity: the modulation of peroxisome proliferator-activated receptor-gamma2 activity as a central mechanism," Bone, vol. 56, no. 2, pp. 255–65, Oct 2013, doi: 10.1016/j.bone.2013.06.016. [PubMed: 23800517]
46. Weiser K, Barton M, Gershoony D, Dasgupta R, and Cardozo T, "HIV's Nef interacts with beta-catenin of the Wnt signaling pathway in HEK293 cells," PLoS One, vol. 8, no. 10, p. e77865, 2013, doi: 10.1371/journal.pone.0077865. [PubMed: 24130899]
47. Baron R and Kneissel M, "WNT signaling in bone homeostasis and disease: from human mutations to treatments," Nat Med, vol. 19, no. 2, pp. 179–92, Feb 2013, doi: 10.1038/nm.3074. [PubMed: 23389618]
48. Mayhew PM et al. , "Relation between age, femoral neck cortical stability, and hip fracture risk," Lancet, vol. 366, no. 9480, pp. 129–35, Jul 9-15 2005, doi: 10.1016/S0140-6736(05)66870-5. [PubMed: 16005335]
49. Fuchs RK, Carballido-Gamio J, Keyak JH, Kersh ME, and Warden SJ, "Physical activity induced adaptation can increase proximal femur strength under loading from a fall onto the greater trochanter," Bone, vol. 152, p. 116090, Nov 2021, doi: 10.1016/j.bone.2021.116090. [PubMed: 34175500]
50. Hazrati Marangalou J, Ito K, Taddei F, and van Rietbergen B, "Inter-individual variability of bone density and morphology distribution in the proximal femur and T12 vertebra," Bone, vol. 60, pp. 213–20, Mar 2014, doi: 10.1016/j.bone.2013.12.019. [PubMed: 24370733]

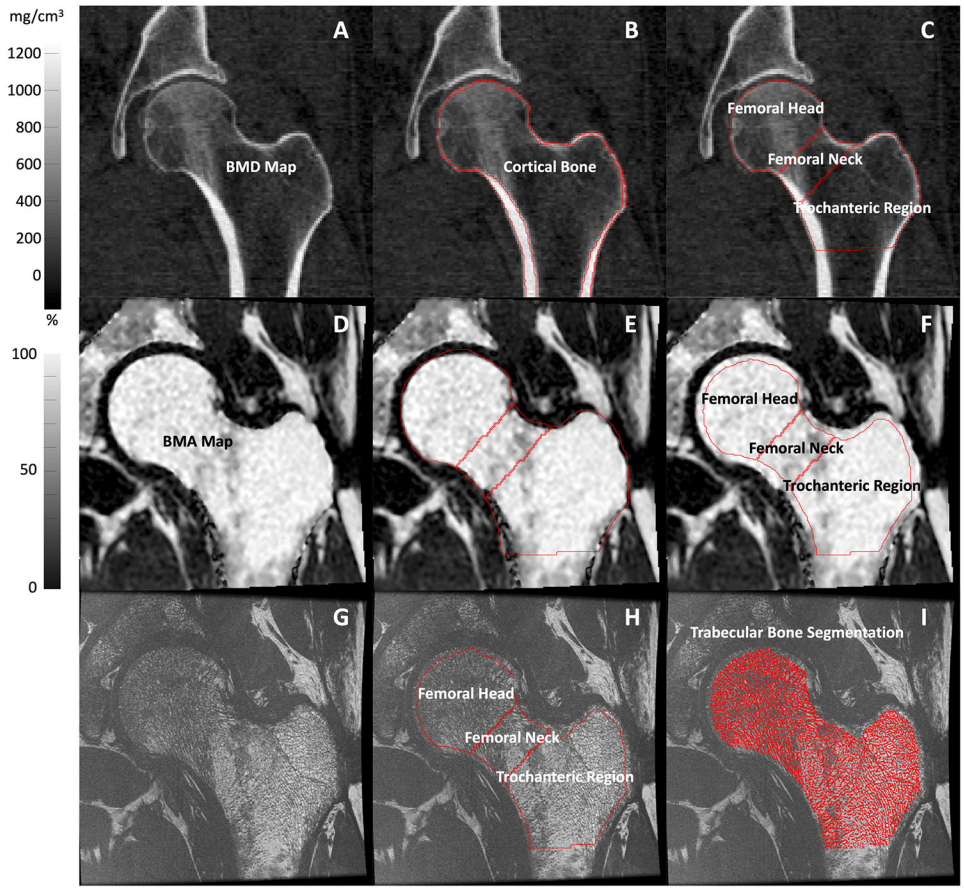

Figure 1.

Representative coronal reformation of a QCT vBMD map of the proximal femur (A) with its periosteal and endosteal boundaries (B), and volumes of interest (C). Representative coronal slice of an MRI BMA map of the proximal femur (D) with the QCT volumes of interest before (E) and after removing a dilated version of the QCT cortical bone segmentation (F). Representative coronal slice of a high-spatial resolution MR image for trabecular bone microarchitecture assessments (G) with the QCT volumes of interest excluding a dilated version of cortical bone (H), and its corresponding trabecular bone segmentation (I).

Table 1.

Participant characteristics

	SN controls	PLWH	*P*-value
n	26	40	
Age (years)	57 (50-67)	58 (50-69)	0.664
Height (cm)	168.45 (146.50-180.10)	170.35 (155.50-193.40)	0.147
Weight (kg)	70.30 (48.80-104.60)	75.40 (54.00-112.60)	0.090
BMI (kg/m^2)	24.66 (18.22-34.00)	25.85 (20.09-35.61)	0.415
VAT (cm^2)	83.89 (32.09-187.37)	128.50 (40.32-367.80)	**0.024** *a, b, c, d, e*
Ab-SAT (cm^2)	196.11 (57.13-454.68)	237.27 (91.64-551.17)	0.720
Thigh-SAT (cm^2)	63.78 (13.32-125.56)	47.89 (12.99-182.90)	0.270
Normal T-score	12	12	0.295
Osteopenic T-score	12	23	0.325
Osteoporotic T-score	2	4	1.000
Absolute CD4 count (cells/uL)		775.50 (316-1986)	
Sex	14 females	12 females	0.072
Race - White	17	26	1.000
Race - Black	3	9	0.338
Race - Asian	4	1	0.074
Race - Unknown/Not reported	2	4	1.000

Values are reported as median (range) or as number of participants.

Mann-Whitney tests except for T-score levels, sex, and race where Fisher's exact test was used.

$P<0.05$:

[a] In complete set for vBMD comparisons (26 SN Controls, 40 PLWH)

[b] In subset for BMA comparisons (26 SN Controls, 38 PLWH)

[c] In subset for trabecular bone microarchitecture comparisons (20 SN Controls, 33 PLWH)

[d] In subset for partial correlations of BMA with trabecular bone microarchitecture (20 SN Controls, 32 PLWH)

[e] In subset for aBMD comparisons (26 SN Controls, 39 PLWH)

SN = seronegative

PLWH = people living with HIV

BMI = body mass index

VAT = visceral adipose tissue

Ab-SAT = abdominal subcutaneous adipose tissue

Thigh-SAT = thigh subcutaneous adipose tissue

Table 2.

DXA aBMD

	SN controls (n=26)	**PLWH (n=39)**	***P*-value (Difference [95% CI])**
Femoral neck			
aBMD	0.769 ± 0.120 (0.784 ± 0.026)	0.742 ± 0.116 (0.727 ± 0.023)	0.061 (−0.057 [−0.117, 0.003])
Total hip			
aBMD	0.942 ± 0.147 (0.983 ± 0.030)	0.884 ± 0.138 (0.870 ± 0.027)	**0.002** (−0.114 [−0.184, −0.044])

aBMD values are expressed in g/cm^2

Linear regression adjusting for height, sex, race, VAT, and Ab-SAT.

Unadjusted mean and standard deviation values are presented along with their estimated marginal means and standard errors in parentheses.

Adjusted mean differences with [95% confidence intervals (CI)] are presented in parentheses.

SN = seronegative

PLWH = people living with HIV

aBMD = areal bone mineral density

Table 3.

QCT vBMD and cortical bone thickness

	SN controls (n=26)	PLWH (n=40)	*P*-value (Difference [95% CI])
Femoral head			
Tb.vBMD	198.35 ± 24.18 (198.06 ± 5.27)	189.88 ± 21.91 (189.12 ± 4.74)	0.151 (−8.94 [−21.25, 3.37])
Int.vBMD	246.54 ± 37.43 (246.56 ± 8.9)	235.21 ± 38.84 (233.29 ± 8.01)	0.207 (−13.27 [−34.08, 7.54])
Femoral neck			
Tb.vBMD	149.27 ± 36.86 (148.59 ± 8.34)	121.96 ± 34.85 (121.65 ± 7.51)	**0.008** (−26.93 [−46.43, −7.43])
Ct.vBMD	680.14 ± 39.95 (679.35 ± 10.42)	666.13 ± 44.38 (665.42 ± 9.38)	0.257 (−13.93 [−38.30, 10.43])
Int.vBMD	325.45 ± 58.94 (323.96 ± 12.41)	294.12 ± 53.71 (294.61 ± 11.16)	**0.047** (−29.36 [−58.36, −0.36])
Ct.Th	1.509 ± 0.162 (1.53 ± 0.05)	1.533 ± 0.222 (1.51 ± 0.04)	0.840 (−0.01 [−0.01, 0.10])
Trochanteric region			
Tb.vBMD	129.13 ± 32.89 (132.12 ± 7.45)	107.33 ± 30.70 (105.78 ± 6.70)	**0.004** (−26.34 [−43.75, −8.93])
Ct.vBMD	674.68 ±48.67 (675.66 ± 10.67)	661.05 ± 41.91 (659.32 ± 9.60)	0.195 (−16.34 [−41.28, 8.61])
Int.vBMD	286.23 ± 49.38 (290.56 ±10.64)	261.49 ± 43.64 (261.40 ± 9.57)	**0.022** (−29.16 [−54.02, −4.29])
Ct.Th	1.622 ± 0.139 (1.65 ± 0.03)	1.661 ± 0.145 (1.65 ± 0.03)	0.946 (0.003 [−0.08, 0.08])
Total hip			
Tb.vBMD	156.46 ± 28.10 (158.13 ± 6.1)	138.59 ± 25.05 (137.63 ± 5.49)	**0.006** (−20.51 [−34.76, −6.25])
Int.vBMD	275.49 ± 42.98 (277.60 ± 9.54)	255.09 ± 40.51 (254.30 ± 8.58)	**0.041** (−23.30 [−45.60, −1.01])

vBMD values are expressed in mg/cm^3.

Ct.Th values are expressed in mm.

Linear regression adjusting for height, sex, race, VAT, and Ab-SAT.

Unadjusted mean and standard deviation values are presented along with their estimated marginal means and standard errors in parentheses.

Adjusted mean differences with [95% confidence intervals (CI)] are presented in parentheses.

The cortical bone from the femoral head was excluded from the analyses due to its thinness.

SN = seronegative

PLWH = people living with HIV

Tb.vBMD = trabecular volumetric bone mineral density

Int.vBMD = integral volumetric bone mineral density, i.e., cortical and trabecular vBMD

Ct.vBMD = cortical volumetric bone mineral density

Ct.Th = cortical thickness

Table 4.

MRI BMA and trabecular bone microarchitecture

	SN controls (n=26*, n=20**)	PLWH (n=38*, n=33**)	*P*-value (Difference [95% CI])
Femoral head			
BMA	87.71 ± 5.15 (88.97 ± 1.03)	90.63 ± 3.74 (91.63 ± 0.93)	**0.033** (2.67 [0.22, 5.11])
Tb.N	1.670 ± 0.030 (1.666 ± 0.009)	1.677 ± 0.039 (1.660 ± 0.008)	0.598 (−0.005 [−0.02, 0.01])
Tb.Sp	0.329 ± 0.009 (0.331 ± 0.003)	0.329 ± 0.012 (0.333 ± 0.002)	0.405 (0.002 [−0.003, 0.008])
Tb.BVF	0.436 ± 0.008 (0.436 ± 0.002)	0.435 ± 0.009 (0.434 ± 0.002)	0.353 (−0.002 [−0.006, 0.002])
Femoral neck			
BMA	78.12 ± 7.05 (79.48 ± 1.62)	84.46 ± 7.13 (85.46 ± 1.46)	**0.003** (5.97 [2.15, 9.80])
Tb.N	1.626 ± 0.045 (1.613 ± 0.014)	1.600 ± 0.059 (1.575 ± 0.012)	**0.014** (−0.04 [−0.07, −0.008])
Tb.Sp	0.345 ± 0.016 (0.350 ± 0.006)	0.354 ± 0.023 (0.362 ± 0.005)	**0.034** (0.01 [0.001, 0.02])
Tb.BVF	0.421 ± 0.012 (0.419 ± 0.004)	0.418 ± 0.016 (0.415 ± 0.003)	0.270 (−0.004 [−0.01, 0.004])
Trochanteric region			
BMA	80.84 ± 6.86 (81.75 ± 1.52)	83.75 ± 5.93 (85.18 ± 1.37)	0.060 (3.44 [−0.16, 7.03])
Tb.N	1.609 ± 0.033 (1.601 ± 0.014)	1.590 ± 0.061 (1.572 ± 0.012)	0.051 (−0.03 [−0.06, 0.00008])
Tb.Sp	0.343 ± 0.013 (0.347 ± 0.005)	0.352 ± 0.023 (0.360 ± 0.005)	**0.023** (0.01 [0.002, 0.02])
Tb.BVF	0.427 ± 0.011 (0.424 ± 0.004)	0.419 ± 0.016 (0.414 ± 0.003)	**0.011** (−0.01 [−0.02, −0.002])
Total hip			
BMA	83.39 ± 5.78 (84.48 ± 1.22)	86.57 ± 4.66 (87.82 ± 1.10)	**0.024** (3.34 [0.45, 6.22])
Tb.N	1.499 ± 0.049 (1.485 ± 0.017)	1.490 ± 0.064 (1.467 ± 0.015)	0.310 (−0.02 [−0.05, 0.02])
Tb.Sp	0.370 ± 0.016 (0.374 ± 0.005)	0.376 ± 0.022 (0.383 ± 0.005)	0.137 (0.008 [−0.003, 0.02])
Tb.BVF	0.430 ± 0.009 (0.428 ± 0.003)	0.425 ± 0.013 (0.422 ± 0.002)	**0.035** (−0.006 [−0.01, −0.0005])

*n for BMA

**n for trabecular bone microarchitecture

BMA values are expressed in %

Tb.N values are expressed in 1/mm

Tb.Sp values are expressed in mm

Tb.BVF values are unitless

Linear regression adjusting for height, sex, race, VAT, and Ab-SAT.

Unadjusted mean and standard deviation values are presented along with their estimated marginal means and standard errors in parentheses.

Adjusted mean differences with [95% confidence intervals (CI)] are presented in parentheses.

SN = seronegative

PLWH = people living with HIV

BMA = bone marrow adiposity

Tb.N = trabecular number

Tb.Sp = trabecular separation

Tb.BVF = trabecular bone volume fraction

Table 5.

Spearman's rank partial correlations of BMA with trabecular vBMD and bone microarchitecture

	SN controls		PLWH		PLWH vs. SN controls
	ρ (Unadjusted ρ)	***P*-values**	**ρ (Unadjusted ρ)**	***P*-values**	***P*-values**
Femoral head					
Tb.vBMD	−0.620 (−0.547)	**0.005** (**0.004**)	−0.041 (−0.074)	0.828 (0.658)	**0.011** (**0.044**)
Tb.N	−0.175 (−0.206)	0.568 (0.382)	−0.271 (−0.284)	0.191 (0.116)	0.740 (0.787)
Tb.Sp	0.129 (0.150)	0.674 (0.525)	0.251 (0.241)	0.227 (0.183)	0.679 (0.757)
Tb.BVF	−0.294 (−0.250)	0.329 (0.287)	−0.227 (−0.150)	0.276 (0.411)	0.812 (0.734)
Femoral neck					
Tb.vBMD	−0.478 (−0.397)	**0.038** (**0.046**)	−0.424 (−0.452)	**0.017** (**0.005**)	0.705 (0.804)
Tb.N	−0.643 (−0.241)	**0.018** (0.305)	−0.228 (−0.311)	0.274 (0.083)	0.082 (0.802)
Tb.Sp	0.441 (0.230)	0.132 (0.328)	0.202 (0.299)	0.332 (0.097)	0.380 (0.809)
Tb.BVF	−0.346 (−0.164)	0.247 (0.488)	−0.180 (−0.252)	0.389 (0.164)	0.558 (0.763)
Trochanteric region					
Tb.vBMD	−0.238 (−0.374)	0.327 (0.061)	−0.452 (−0.432)	**0.011** (**0.007**)	0.363 (0.794)
Tb.N	−0.050 (−0.158)	0.872 (0.505)	−0.549 (−0.389)	**0.005** (**0.028**)	0.063 (0.410)
Tb.Sp	0.135 (0.147)	0.660 (0.534)	0.585 (0.389)	**0.002** (**0.028**)	0.080 (0.390)
Tb.BVF	−0.085 (−0.229)	0.783 (0.331)	−0.518 (−0.322)	**0.008** (0.073)	0.110 (0.740)
Total hip					
Tb.vBMD	−0.405 (−0.487)	0.085 (0.013)	−0.387 (−0.391)	**0.031** (**0.016**)	0.938 (0.660)
Tb.N	−0.367 (−0.475)	0.217 (**0.036**)	−0.453 (−0.447)	**0.023** (**0.011**)	0.735 (0.907)
Tb.Sp	0.409 (0.526)	0.165 (**0.019**)	0.591 (0.484)	**0.002** (**0.006**)	0.424 (0.852)
Tb.BVF	−0.264 (−0.310)	0.384 (0.184)	−0.543 (−0.334)	**0.005** (0.062)	0.269 (0.929)

26 SN Controls and 38 PLWH for BMA vs. Tb.vBMD.

20 SN Controls and 32 PLWH for BMA vs. trabecular bone microarchitecture.

All partial correlations adjusted for height, sex, race, VAT, and Ab-SAT.

Unadjusted Spearman correlations and their corresponding *P*-values are presented in parentheses.

Differences in the strength of correlation coefficients were assessed using the Fisher's z transformation.

SN = seronegative

PLWH = people living with HIV

BMA = bone marrow adiposity

Tb.vBMD = trabecular volumetric bone mineral density

Tb.N = trabecular number

Tb.Sp = trabecular separation

Tb.BVF = trabecular bone volume fraction